Journal of Engineering and Technological Sciences

Research Paper

Evaluation of Crash Energy Management of the First-Developed High-Speed Train in Indonesia

Karisma Rizal[1,2] & Achmad Syaifudin[3,*]

[1]Graduate School of Mechanical Engineering, Institut Teknologi Sepuluh Nopember (ITS), Kampus Keputih, Surabaya 60111, Indonesia
[2]Department of Design, Technology Division, PT. Industri Kereta Api (PT. INKA), Jalan. Yos Sudarso No.71, Madiun 63122, Indonesia
[3]Laboratory of Solid Mechanics, Department of Mechanical Engineering, Institut Teknologi Sepuluh Nopember (ITS), Kampus Keputih, Surabaya 60111, Indonesia

Corresponding author: saifudin@me.its.ac.id

Abstract

Crash energy management is an essential evaluation stage of passive safety systems for high-speed trains. As a part of crash energy management, crash energy absorption has been researched for the last decade. The development of its components has also been performed individually. This paper presents a numerical analysis of the configuration of an energy absorption system for high-speed trains developed in Indonesia. Three placement configurations of the energy absorption system were investigated using explicit dynamic analysis in ANSYS. Total energy absorption, deceleration pulse, and deformation length were considered in the evaluation of the numerical analysis results. The collision criteria used in this study were according to EN 15227 and CFR 238 standards. This study revealed that the existing design could fulfill the energy absorption and average deceleration pulse required by EN 15227. Nevertheless, the existing design could not fulfill the energy absorption and maximum deceleration pulse required by CFR 238. It was also indicated that by positioning the anti-climber slightly forward, changing the deformation force of the crush box, and adding an impactor, the quality of energy absorption and average deceleration pulse could be improved.

Keywords: *crashworthiness; crash energy management; deceleration pulse; high-speed train; occupant protection.*

Introduction

Indonesia's research and innovation agency (BRIN) has collaborated with the first fully integrated rolling stock manufacturer in Southeast Asia, PT. INKA, to develop a high-speed train. This development marks a significant transition from conventional trains that have been operational in Indonesia to the introduction of high-speed trains. While conventional trains have a maximum speed of 100 km/h, the planned operating speed for these high-speed trains is 250 km/h. The heightened speed necessitates an enhanced safety system, as the risk of accidents escalates with increased train speed. Train safety systems can be categorized into two types: active safety systems and passive safety systems. Active safety systems are designed to prevent train accidents by automatically halting the train in emergencies, such as lack of driver response, earthquakes, train disconnections, etc. Furthermore, active security systems can disengage train traction in case of system failures, such as doors not closing properly, brakes being constantly active, insufficient compressed air pressure, over-speed conditions, and others. Extensive research has been conducted on active safety systems, encompassing signaling transmission system [1], accurate positioning techniques [2], and operation control systems [3]. Various countries have developed and named their own active security systems, such as ATP (Automatic Train Protection) in Indonesia, ATC (Automatic Train Control) in Japan, ACSES (Advanced Civil Speed Enforcement System) in the USA, and others[4]. On the other hand, the passive safety system aims to mitigate damage and ensure passenger safety in the event of an accident when the active safety system fails to prevent an accident.

One of the passive safety systems employed in trains is the crashworthiness of their structures. Crashworthiness serves two primary functions, namely crash management and occupant protection. Crash management refers

ISSN: 2337-5779
J. Eng. Technol. Sci. Vol. 55, No. 3, 2023, 235-246
DOI: 10.5614/j.eng.technol.sci.2023.55.3.2

to a train's ability to systematically absorb impact energy during a collision, thereby averting various failure patterns such as lateral buckling and overriding. Next, occupant protection ensures passengers are protected from collision-related impacts. In high-speed trains, collision energy is absorbed by a designated energy-absorbing module known as the Crash Energy Management (CEM) module. Comprising multiple energy-absorbing sub-components, the CEM module efficiently dissipates impact energy in a predetermined order. Research into crashworthiness capabilities at the sub-component scale, encompassing items like single steel tubes [5], honeycomb structure crash boxes [6], foam-filled crash boxes [7], and expanded metal tubes [8], has been extensive. Crashworthiness analyses for conventional trailer trains in Indonesia have already been undertaken, including studies on passenger cars [9], passive safety K1 passenger cars [10], and passenger trains [11]. In the case of conventional trains, impact energy is absorbed directly into the main frame incorporating embedded CEM components. Meanwhile, multiple-unit trains featuring cabin cars integrate a CEM module at the front of the cabin car to absorb initial impact energy produced at the first hit. In Indonesia, research into CEM components within cabin cars has already been available, albeit limited to medium-speed trains [12]. Nevertheless, no study has yet addressed this aspect in the context of high-speed trains.

The configuration of energy-absorbing sub-components within the CEM module holds significant importance. This pertains to the collision sequence and energy absorption, which collectively ensure favorable deformation performance, optimal energy absorption, and safe deceleration for passengers. This study evaluates the performance of an existing CEM module design, jointly developed by BRIN and PT. INKA. Moreover, various design variations were reviewed, considering factors such as deformation, force response, energy absorption, and deceleration pulse. Simulation conditions and safety criteria were evaluated following the BS EN 15227 (2008) [13] and CFR Part 238 (2020) [14] standards. The selection of BS EN 15227 (2008) stemmed from its adaptation as the crashworthiness standard in Indonesia, although it does not classify trains based on speed. For comparison purposes, the CFR standard was incorporated as a specific benchmark for high-speed train crashworthiness, aligning with the intended application of this model in the context of high-speed trains. Throughout this investigation, numerical simulation was leveraged to its fullest extent in the comparison of several model variations. The simulation outcomes include deformation manner, energy absorption, and deceleration pulse profiles. Unfortunately, experimental studies were hindered by limited testing facilities at this time and will be carried out for future studies.

Crash Energy Management

Structure Description

The CEM module design for the high-speed train comprises a frame and three energy-absorbing components, namely a coupler with a deformation tube, an anti-climber with a buffer, and a crash box, as depicted in Figure 1. The coupler with a deformation tube features a coupler suspension responsible for regular operation and a deformation tube that activates during crash scenarios. In CEM structures, an anti-climber, consisting of a tooth profile, is employed to prevent train overriding behavior. Additionally, a buffer is utilized to absorb kinetic energy during crashes. The coupler's graphic force and the anti-climber's specification are provided in Figure 2(a) and (b), respectively. Both component specifications were provided by PT. INKA's supplier. In the simulation model, the geometries of the coupler and the anti-climber remain consistent across all design variations. The existing design incorporates a crash box with a deformation force surpassing that of the coupler. Variation A uses a crash box with a lower deformation force than the coupler and positions the anti-climber slightly forward. Variation B, similar to the existing design, employs a crash box with a higher deformation force than the coupler, but positions the anti-climber slightly forward and introduces an impactor frame as well, as shown in Figure 3.

DOI: 10.5614/j.eng.technol.sci.2023.55.3.2

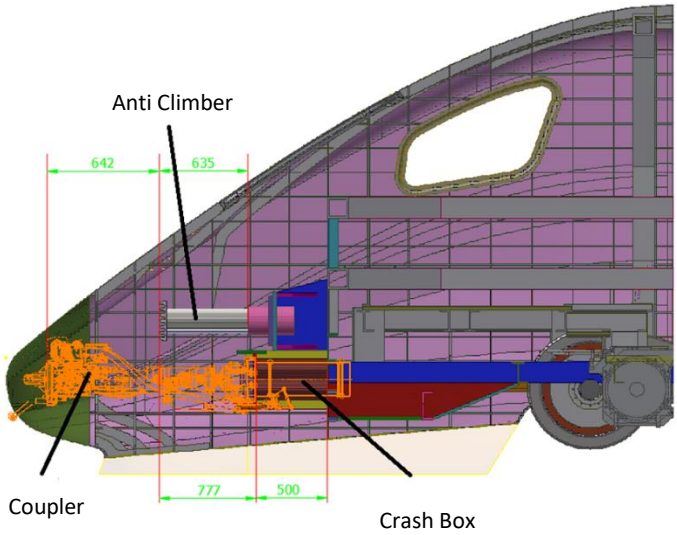

Figure 1 CEM design of the high-speed train.

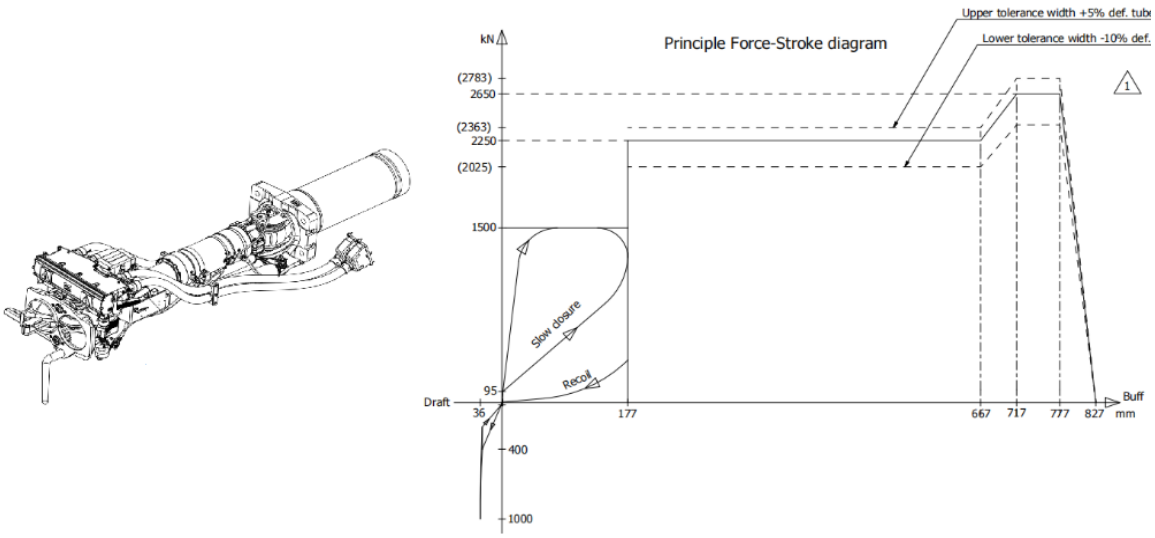

(a)

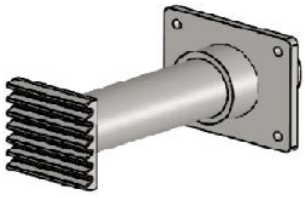

Energy storing capacity (E)	: 760 kJ. 10%
Maximum dynamic reaction (Rdy)	: 1400 kN ± 15%
Stroke	: 635 mm
Utilization temperature	: -50 C, +70 C

(b)

Figure 2 (a) Coupler with deformation tube, (b) anti-climber with buffer (Personal communication with PT INKA).

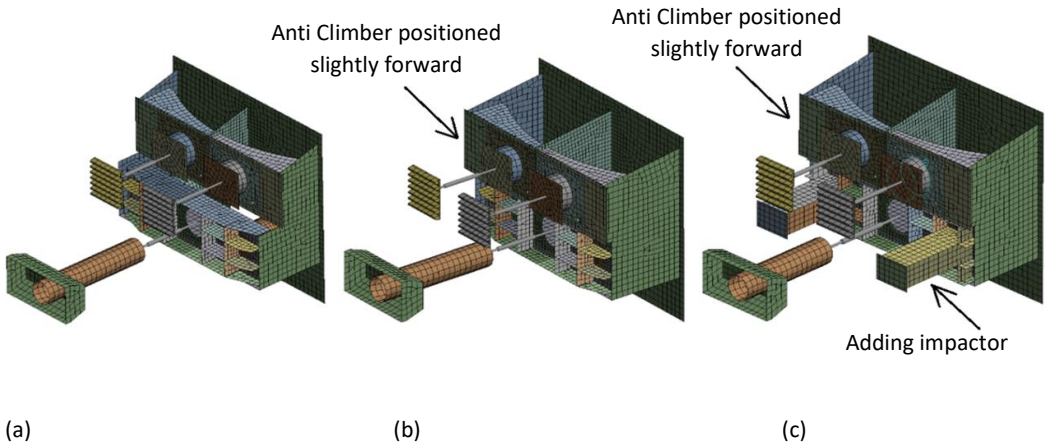

Figure 3 Variations of CEM module: (a) existing design, (b) variation A, and (c) variation B.

Finite Element Modeling

Pre-Processing

The crashworthiness analysis for the crash energy management of the high-speed train was modeled using Ansys 19 with the LS-Dyna solver. As depicted in Figure 4, a point mass was connected to the CEM frame with a value of 46 tons. In the simulation, the structure collides with a rigid wall, where the rigid wall serves as an idealized symmetric collision representation with simplifications [15]. The mesh used was a linear-map type, employing four-node shell elements. The section utilized a Belytschko–Tsay element formulation with three integral points in the material's thickness direction and one integral point in the plane element [16].

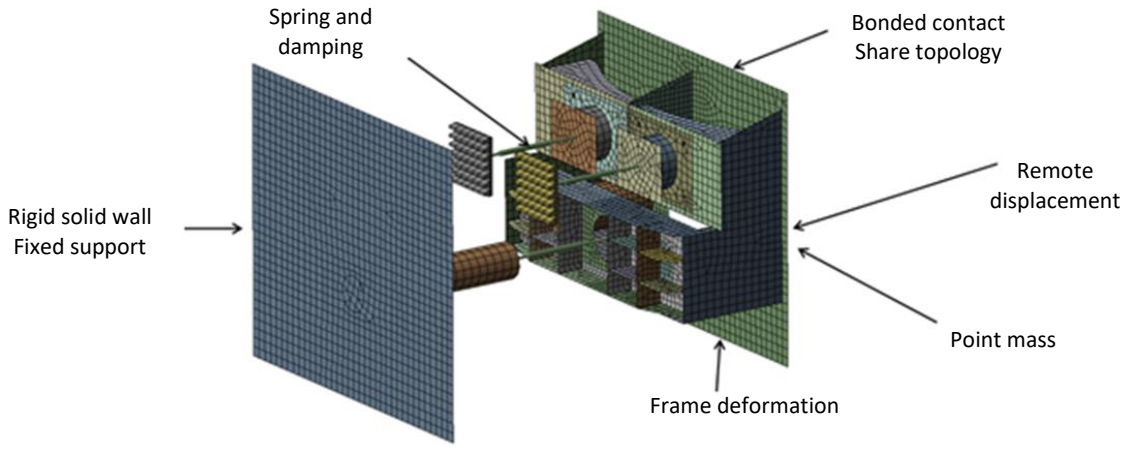

Figure 4 Boundary condition used in the simulation.

Processing

The model material for the crash energy management frame and the crash box was isotropic elasticity, chosen to define the elastic-plastic properties of the materials. Then Johnson-Cook strength was selected to define the material properties at high strain rates. The chosen material was aluminum 6005A-T6, with the corresponding parameters detailed in Table 1[17]. The frame's stiffness behavior was modeled as flexible, while the rigid wall stiffness was defined as rigid. The structural frame was connected using bonded contact and shared topology. The coupler with the deformation tube and the buffer of the anti-climber were modeled using a damper model. Two crash velocities were incorporated: the first at 10 m/s (equivalent to 36 km/h) in line with BS EN 15227

DOI: 10.5614/j.eng.technol.sci.2023.55.3.2

(2008) [13], and the second at 14.75 m/s (or 53 km/h) to meet the 5 MJ energy absorption requirement specified in CFR Part 238 (2020) [14]. To prevent deformation modes with spurious zero energy, Hourglass control type 4, known as 'Flanagan-Belytschko Stiffness Form', was utilized, employing an hourglass coefficient of 0.04[16].

Table 1 Material properties of Aluminium 6005A-T6 [17].

Parameter	Value	Unit
Density (ρ)	2700	Kg/m^3
Tensile yield strength	230	MPa
Tensile ultimate strength	280	MPa
Poisson ratio (v)	0.3	-
Modulus elasticities (E)	70	GPa
Initial yield stress (A)	270	MPa
Hardening constant (B)	134	MPa
Strain hardening coefficient (n)	0.514	-
The strain rate constant (C)	0.0082	-
Thermal softening exponent (m)	0.703	-
Melting temperature (TM)	893	K
Room temperature (TR)	293	K
Reference strain rate (epso)	0.001	/Sec
Specific heat (cp)	910	J/kg. K
Failure parameter 1 (D1)	0.06	-
Failure parameter 2 (D2)	0.497	-
Failure parameter 3 (D3)	-1.551	-
Failure parameter 4 (D4)	0.0286	-
Failure parameter 5 (D5)	6.8	-

Verification

To ensure the accuracy of the numerical simulation, each chosen constant, and the meshed finite element model were meticulously verified. Additionally, the simulation results were validated through an experimental study. In this context, the simulation's accuracy was affirmed by scrutinizing all input data for correctness, evaluating the quality of the meshed model, and assessing the stability of the energy balance.

Table 2 summarizes the mesh quality of the FE model. Both the maximum and minimum mesh quality fell within the acceptable range defined by ANSYS Guide [18].This signifies that the mesh number's influence on the simulation result is negligible. For this research, the aspect ratio was at a maximum of 4.1 and an average of 1.2, both of which are well within the acceptable range of less than 8. Skewness, which indicates how closely a face or cell approaches the ideal shape, follows a 'lower is better' rule in terms of value.

Table 2 Mesh quality.

Parameter	Max Value	Min Value	Average Value	Acceptable Value	Remark
Aspect ratio	4.1	1	1.20	1 to 10	GOOD
Skewness	0.7	0	0.06	0 to 0.8	GOOD
Jacobian ratio	1	0.44	0.95	-1 to 1	GOOD
Orthogonal quality	1	0.62	0.98	0.2 to 1	GOOD

The skewness value of the research model in this study fell within the criteria for good-quality models, with a maximum of 0.7 and an average of 0.06. The Jacobian ratio indicates the mapping between element space and real space. Higher Jacobian ratios suggest a more unreliable computational simulation. A favorable Jacobian ratio typically ranges between -1 and 1. For this research, the Jacobian ratio reached a maximum of 1, with an average of 0.95. The orthogonal quality scale ranges from 0 to 1, with 0 representing the least desirable outcome and 1 representing the most favorable result. In this study, the minimum orthogonal quality value was 0.62, while the average was 0.98. Both values align with the acceptable range of 0.2 to 1.

Presented in Figure 5 are graphics depicting grid independency concerning variations in mesh size, ranging from 30 mm to 70 mm. The average force result exhibited a decrease with increasing mesh size. Based on the simulation results, meshes under 40 mm displayed a gently sloping trend with an error rate of less than 5%. Thus, a mesh size of 30 mm was selected due to its commendable accuracy, featuring an error of only 0.5%, while maintaining a reasonable iteration time. Hourglass energy represents the work performed by forces to counteract hourglass modes - non-physical distortion modes yielding zero strain and stress. A smaller hourglass energy indicates improved energy balance within the simulation. Typically, this value is maintained below 10% of the total energy [19]. In the context of this research, the energy error represented by the hourglass energy was just 1%, equivalent to 50 kJ out of the total energy 5,000 kJ.

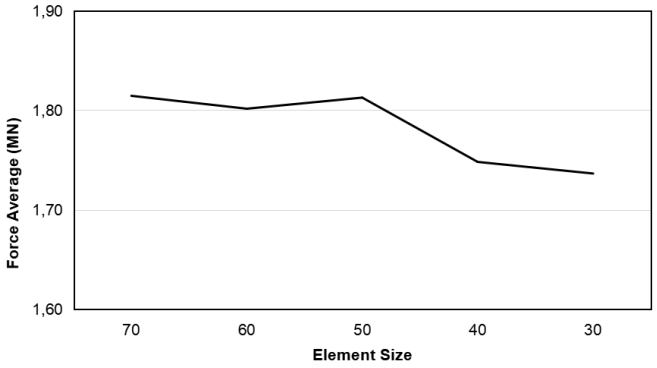

Figure 5 Grid independency.

Results and Discussion

Deformation

As shown in Figure 6(a), the existing design exhibited a maximum deformation of 1,238.8 mm. Kinetic energy was absorbed through the functioning of the coupler with the deformation tube and the anti-climber with buffer. The coupler with the deformation tube underwent complete deformation until it reached its maximum absorption capacity. In contrast, the anti-climber with buffer experienced partial deformation, effectively absorbing a portion of the kinetic energy, which is evident from the reduced length of the damping model. However, the crash box displayed no deformation; its length remained unchanged, and therefore, it did not contribute to kinetic energy absorption.

The maximum deformation of design variation A was measured at 1,006.6 mm, as shown in Figure 6(b). All energy-absorbing components collaborated, as can be seen from the length of deformation. However, the deformed length did not reach its maximum extent, implying that the absorption capacity of the three energy-absorbing components was not fully utilized.

Depicted in Figure 6(c), design variation B exhibited a maximum deformation of 893.8 mm. The coupler with the deformation tube effectively absorbed energy until it nearly reached the deformation length limit. The the damping model's length for the anti-climber with buffer appeared to be reduced; however, the anti-climber component did not come into direct contact with the solid wall. This indicates a backward displacement due to the collision's reaction force. The crash box experienced a slight deformation, suggesting that it possessed sufficient stiffness to absorb residual kinetic energy when the crash box's impactor came into contact with the solid wall.

DOI: 10.5614/j.eng.technol.sci.2023.55.3.2

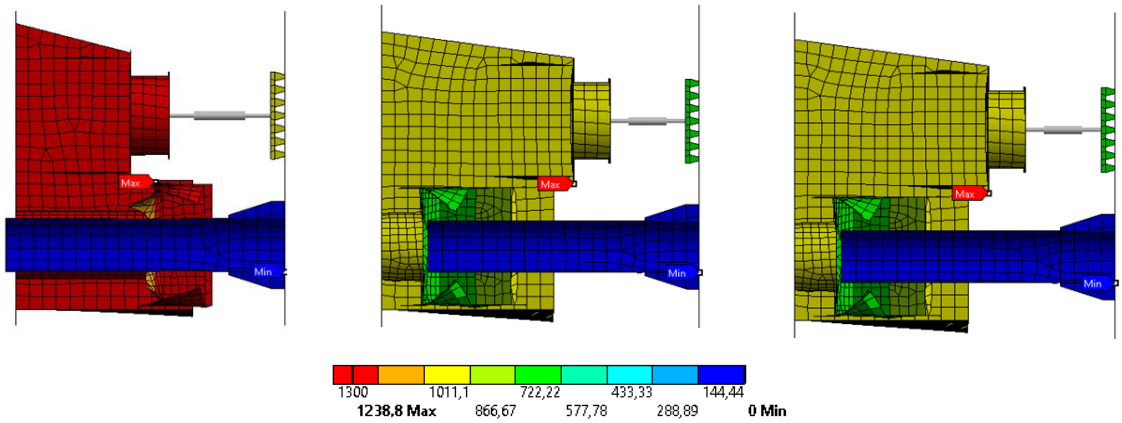

(a) (b) (c)

Figure 6 Deformation of CEM at a collision speed of 10 m/s for: (a) existing design, (b) variation A, and (c) variation B.

As shown in Figure 7, the maximum deformation of the CEM module at a collision speed of 14.75 m/s for (a) the existing design, (b) variation A, and (c) variation B was 1419.9 mm, 1515.6 mm, and 1218.1 mm respectively. Depicted in Figure 7(a), the coupler with the deformation tube underwent complete deformation in the existing design. Although the damping model's length for the anti-climber with buffer was reduced, the anti-climber component did not make direct contact with the solid wall. In this scenario, the CEM frame collided with the solid wall once the coupler with the deformation tube's absorption capacity was exhausted, leading to the detachment of the coupler from the frame. Subsequently, the CEM frame absorbed the remaining kinetic energy before absorption function B was reached, and there was a backward displacement due to the reaction force from the collision. The coupler with the deformation tube, the anti-climber with buffer, and the crash box experienced complete deformation and each reached their absorption capacity, as shown in Figure 7(b). The visibly deformed CEM frame indicates the presence of residual kinetic energy that impacted the frame, surpassing the energy-absorbing components' absorption capability.

As shown in Figure 7(c), design variation B exhibited the shortest deformation length. Both the coupler with the deformation tube and the anti-climber with buffer achieved their maximum deformation length and absorption capacity. Then, the remaining kinetic energy was absorbed by the crash box, causing it to deform until the simulation concluded. Interestingly, the anti-climber remained unaffected, meaning that once the collision ceased, a backward displacement occurred due to the reaction force.

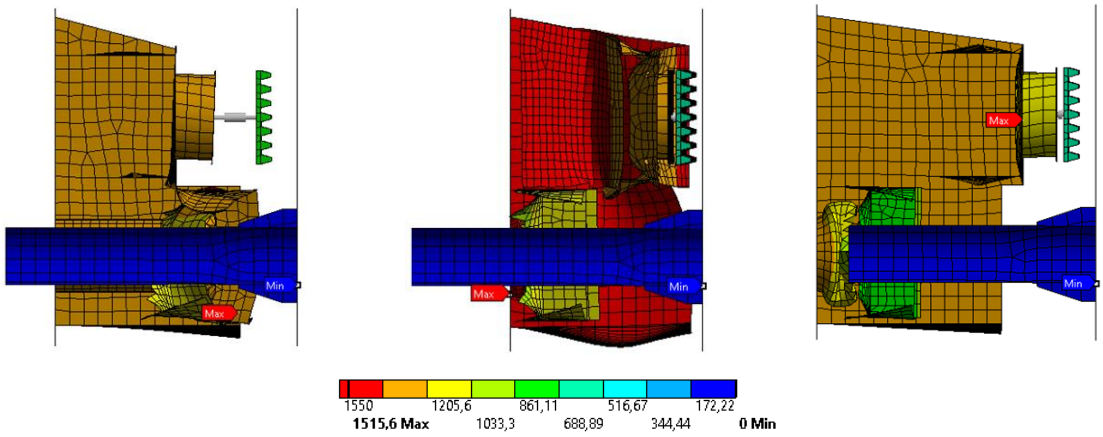

(a) (b) (c)

Figure 7 Deformation of the CEM module at a collision speed of 14.75 m/s for: (a) existing design, (b) variation A, and (c) variation B.

Energy Absorption

Figure 8 displays a graphic representing the kinetic energy for a collision speed of 10 m/s. The Y-axis shows the value of the kinetic energy in kJ, and the X-axis shows the time duration in ms. Initially, the kinetic energy experienced a decrease at the onset of the collision, exhibiting a similar trend across all three design variations. The kinetic energy in design variations A and B continued to decline until 160 ms and reached 0 kJ, indicating the completion of the collision. The graphic trend of kinetic energy at 90 ms to 130 ms of the existing design looks sloping, implying that there was no absorption of energy during that time. Although the kinetic energy in the existing design began to fall again at 130 ms, it did not reach the 0-kJ threshold by the end of the simulation. The total energy absorbed at a collision speed of 10 m/s for the existing design, variation A, and variation B after 200 ms simulation time was 2212 kJ, 2292 kJ, and 2297 kJ, respectively. Notably, all design variations demonstrated energy absorption capabilities that aligned with the collision criteria based on the BS EN 15227 (2008) standard [13].

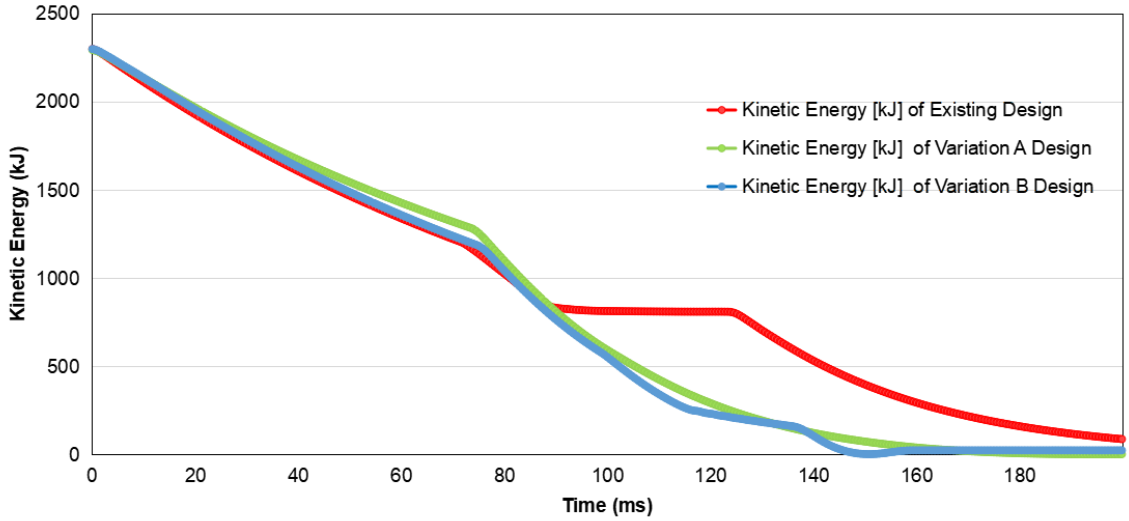

Figure 8 Kinetic energy at a collision speed of 10 m/s.

A graphic representing the kinetic energy for a collision speed of 10 m/s is presented in Figure 9. The Y-axis depicts the value of kinetic energy in kJ, and the X-axis shows the time duration in ms. A consistent trend of kinetic energy decrease is observed at the outset of the collision. Design variation A showed higher kinetic energy at 30 ms compared to the other design variations. This higher value for variation A persisted until the completion of the simulation, indicating a lower energy absorption ability compared to the other design variations. Next, the graphic trend of the existing design between 50 ms and 70 ms appears sloping, signifying negligible energy absorption during that period. While the kinetic energy of the existing design initially follows a slope similar to the beginning of the simulation, a very steep decline is evident in the kinetic energy graph from 70 ms to 100 ms, indicating substantially high energy absorption during that interval.

The total energy absorption at a collision speed of 14.75 m/s, after 200ms of simulation time, was 4,999 kJ for the existing design, 4,987 kJ for variation A, and 4,999kJ for variation B. The total energy absorption of design variation B satisfied the CFR Part 238 (2020) standard [14], by achieving 5 MJ energy absorption. As depicted in Figure 8, residual kinetic energy was absorbed by the CEM frame when the absorption components' ability was exhausted. In comparison to a conventional train [20], the CEM module's energy absorption characteristic showed a similar trend, characterized by the gradual energy absorption curve and the zero crash energy at the end of the collision.

DOI: 10.5614/j.eng.technol.sci.2023.55.3.2

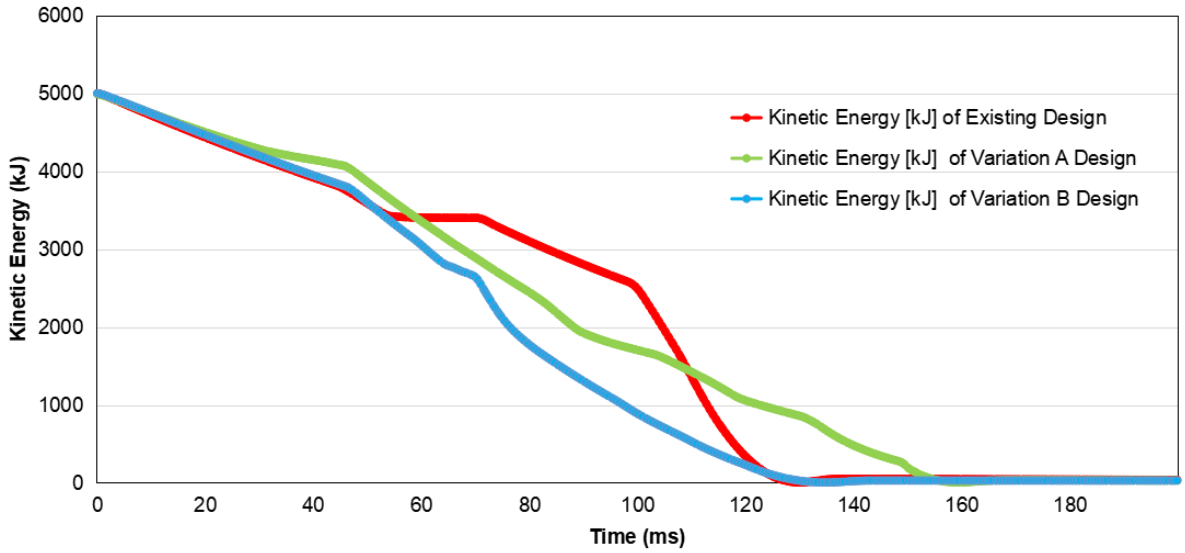

Figure 9 Kinetic energy at a collision speed of 14.75 m/s.

Deceleration Pulse

The higher the deceleration pulse, the greater the danger to passenger safety [21]. Figure 10 illustrates the deceleration pulse graphic for a collision speed of 10 m/s. The Y-axis shows the value of the deceleration pulse in g, and the X axis shows the time duration in ms. The graphic depicts a consistent trend from the beginning of the collision until 70 ms when the coupler with the deformation tube worked to absorb the kinetic energy. The deceleration pulse increased when the deformation tube reached the end of its stroke. Between 90 ms and 120 ms, the existing design's deceleration pulse dropped to zero, indicating no deceleration was applied to the CEM module and no energy was absorbed during that period.

The deceleration pulse of the existing design increased at 120 ms as the anti-climber with buffer made contact with the solid wall, maintaining a sloping trend until the conclusion of the collision. Design variation A experienced an increased deceleration pulse at 70 ms, peaking at 10.3 g, and gradually decreasing thereafter until the collision ended. Conversely, the deceleration pulse of design variation B increased sharply at 130 ms and reached its peak deceleration at 21 g when the impactor of the crash box contacted the solid wall. This pulse then decreased sharply as the kinetic energy depleted. The average deceleration pulse for a collision speed of 10 m/s during the 200 ms simulation time was 4 g for the existing design, 5.4 g for design variation A, and 6.4 g for design variation B.

The existing design met the average deceleration pulse requirement of the BS EN 15227 (2008) standard [13], but the crash box did not engage. Both design variations A and B exceeded the required deceleration pulse. Comparatively, the CEM's deceleration pulse was lower than that of a conventional train's crashworthiness [11] because the crash force impacted the CEM module before the main frame, while in the conventional design, the crash force directly hit the mainframe.

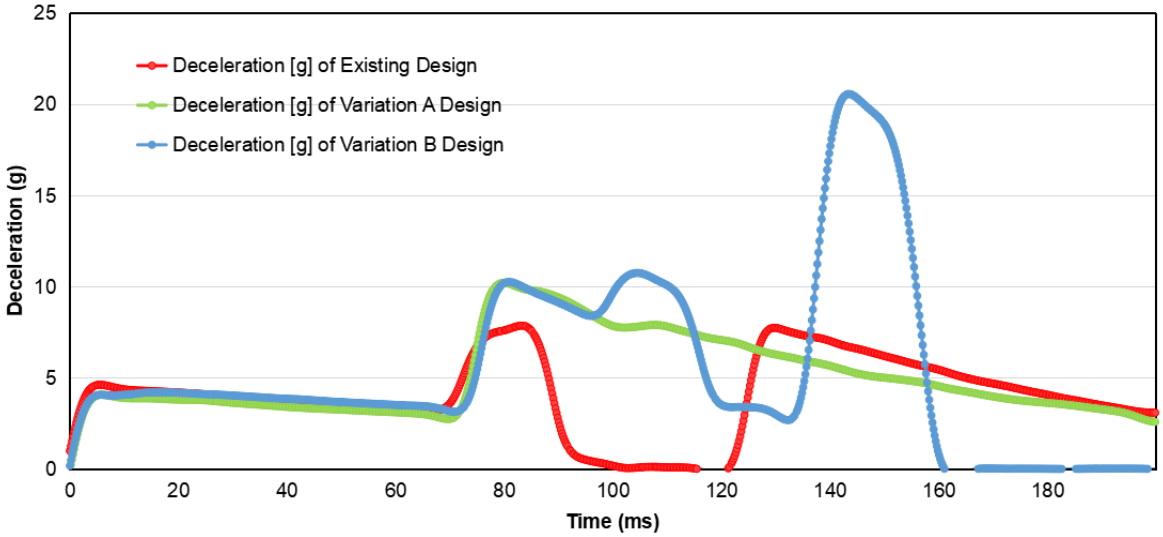

Figure 10 Deceleration pulse at a collision speed of 10 m/s.

Figure 11 shows the graphic of the deceleration pulse for a collision speed of 14.75 m/s. The Y-axis shows the value of the deceleration pulse in g, and the X-axis shows the time duration in ms. From the commencement of the collision until 40 ms, the deceleration maintained a consistent graphic trend across all design variations. The existing design's CEM frame began to collide with the coupler head, which directly contacted the solid wall at 100 ms, significantly increasing the deceleration pulse and reaching a very high peak deceleration at 40 g. The existing design reached its peak when the CEM frame directly impacted the solid wall, and due to the CEM frame's high rigidity, the deceleration became very high. After reaching its peak, the deceleration fell to zero, indicating that the collision's termination. Next, design variation B had a fluctuating deceleration value during the collision, but at the end of the collision, at 145 ms, the deceleration experienced a sharp increase and reached its peak at 34 g. The increase in the deceleration pulse for design variation A was caused by the residual kinetic energy of design variation A hitting the CEM frame at the end of the collision when the energy-absorbing components reached the limit of their absorption capacity. The deceleration pulse of design variation B also fluctuated throughout the collision and had a lower peak deceleration pulse of 23 g compared to the other variations. The maximum deceleration pulse at a collision speed of 14.75 m/s for all design variations could not fulfill the 8 g maximum deceleration pulse requirement stipulated by the CFR Part 238 (2020) standard [14].

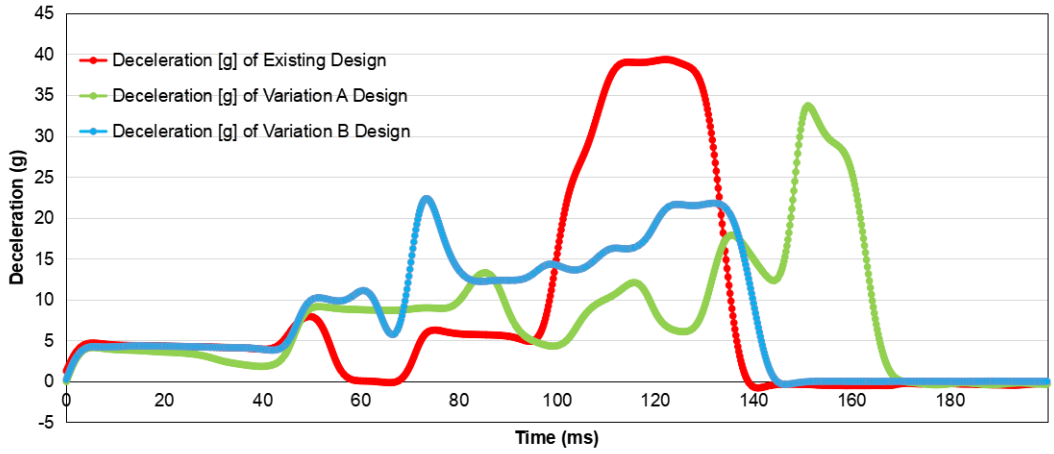

Figure 11 Deceleration pulse at a collision speed of 14,75 m/s.

DOI: 10.5614/j.eng.technol.sci.2023.55.3.2

Conclusion

The existing design met the energy absorption and average deceleration pulse requirements determined by the BS EN 15227 (2008) standard, but the crash box did not work properly because the stiffness of the crash box was higher than that of the coupler's deformation tube. The existing design was unable to fulfill the 5 MJ energy absorption and maximum deceleration pulse required by the CFR Part 238 (2020) standard, as the crash box failed to absorb energy, resulting in the residual energy directly impacting the CEM frame.

Variation A managed to meet the energy absorption required by BS EN 15227 (2008). Nonetheless, it exceeded the limit for average deceleration. Both the energy absorption and maximum deceleration required by CFR Part 238 (2020) could not be fulfilled by design variation A due to insufficient energy absorption in the crash box, leading to the residual kinetic energy hitting the CEM frame and increasing the deceleration pulse.

Variation B was able to satisfy the energy absorption criteria outlined by both BS EN 15227 (2008) and CFR Part 238 (2020). However, neither the average deceleration nor the maximum deceleration requirements were met. By incorporating a highly rigid crash box and an additional impactor, the functionality of the crash box could be optimized to maximize energy absorption and enhance the deceleration pulse.

Acknowledgments

The authors are greatly appreciative of the support provided by PT. INKA and BRIN, including the provision of specification data and model geometry. The authors also gratefully acknowledge the financial support from Institut Teknologi Sepuluh Nopember (Sepuluh Nopember Institute of Technology) for this work, under the Publication Writing and IPR Incentive Program (PPHKI) 2023 project scheme.

References

[1] Mochizuki, H., Takahashi, S., Nakamura, H., Nishida, S. & Ishikawa, R., *Development of a High-speed Rail Transmission System Using Digital Signal Processors for Railway Signalling*, WIT Transactions on the Built Environment, **103**, pp. 295-304, August. 2008.

[2] Chen, D., Wang, L. & Li, L., *Position Computation Models for High-speed Train based on Support Vector Machine Approach*, Applied Soft Computing Journal, **30**, pp. 758-766, May. 2015.

[3] Ai, B. et al., *Challenges toward Wireless Communications for High-speed Railway*, IEEE Transactions on Intelligent Transportation Systems, **15**(5), pp. 2143-2158, Oct. 2014.

[4] Wikipedia, *Train Protection System*, Wikimedia Foundation, https://en.wikipedia.org/wiki/Train_protect-ion _system, (02 October 2022).

[5] Velmurugan, R. & Muralikannan, R., *Energy Absorption Characteristics of Annealed Steel Tubes of Various Cross Sections in Static and Dynamic Loading*, Latin American Journal of Solids and Structures, **6**(4), pp. 385-412, January. 2009.

[6] Choiron, M.A., *Characteristics of Deformation Pattern and Energy Absorption in Honeycomb Filler Crash Box due to Frontal Load and Oblique Load Test*, Eastern-European Journal of Enterprise Technologies, **2**(7) (104), pp. 6-11, April. 2020.

[7] Toksoy, A.K. & Güden, M., *The Optimisation of the Energy Absorption of Partially Al Foam-filled Commercial 1050H14 and 6061T4 Al Crash Boxes*, International Journal of Crashworthiness, **16**(1), pp. 97-109, April. 2011.

[8] Nouri, M.D., Hatami, H. & Jahromi, A.G., *Experimental Investigation of Expanded Metal Tube Absorbers under Axial Impact Loading*, Structural Engineering & Mechanics, **54**(6), pp. 1245-1266, January. 2015.

[9] Setiawan, R. & Pamintori, M., *Crashworthiness Analysis of Indonesian Passenger Train Structures*, Seminar Nasional Tahunan Teknik Mesin, pp. 191-195, 2017. (Text in Indonesian)

[10] Dharma, I.G.S.S., Suweca, I.W. & Setiawan, R., *Basic Design of Passive Safety System for Class 1 Passenger Trains (K1 Trains),* Seminar Nasional Tahunan Teknik Mesin, pp. 889-896, 2016. (Text in Indonesian)

[11] Setiawan, R., Handoko, Y.A., Ramadhan, F.I. & Fahmi, M.Y., *Design and Analysis of Impact Energy Absorption in the Crash Zone of the National Passenger Train Area*, Seminar Nasional Tahunan Teknik Mesin, pp. 1-8, 2019. (Text in Indonesian)

[12] Syaifudin, A., Windharto, A., Setiawan, A. & Farid, A.R., *Energy Absorption Analysis on Crash-Module Shape and Configuration of Medium-Speed Train*, Lecture Notes in Electrical Engineering, **876**, pp. 171-179, 2022.
[13] BS EN15227 - *Railway Applications in Crashworthiness Requirements for Railway Vehicle Bodies*, 2008.
[14] 49 CFR Part 238, *Passenger Equipment Safety Standards*, Code of Federal Regulations (CFR), US, 4. 2020.
[15] Kirkpatrick, S.W., Schroeder, M. & Simons, J.W., *Evaluation of passenger rail vehicle crashworthiness*, International Journal of Crashworthiness, **6**(1), pp. 95-106, January. 2001.
[16] Wang, S., Peng, Y., Wang, T., Che, Q. & Xu, P., *Collision Performance and Multi-objective Robust Optimization of a Combined Multi-cell thin-walled Structure for High-speed train*, Thin-Walled Structures, **135**, pp. 341-355, February. 2019.
[17] Børvik, T., Clausen, A.H., Eriksson, M., Berstad, T., Hopperstad, O.S. & Langseth, M., *Experimental and Numerical Study on the Perforation of AA6005-T6 Panels*, Int J Impact Eng, **32**(1-4), pp. 35-64, December. 2005.
[18] ANSYS Guide, *Introduction to ANSYS Meshing*, 2015.
[19] Bala, S. & Day, J., *General Guidelines for Crash Analysis in LS-DYNA ® Modeling Guidelines for Crash Analysis*, 2003.
[20] Zhu, T., Xiao, S.N., Hu, G.Z., Yang, G.W. & Yang, C., *Crashworthiness Analysis of The Structure of Metro Vehicles Constructed from Typical Materials and the Lumped Parameter Model of Frontal Impact*, Transport, **34**(1), pp. 75-88, January. 2019.
[21] Severson, K.J., Parent, D.P. & Tyrell, D.C., *Two-Car Impact Test of Crash-Energy Management Passenger Rail Cars: Analysis of Occupant Protection Measurements*, Rail Transportation, pp. 87-96, January. 2004.

Manuscript Received: 3 October 2022
Revised Manuscript Received: 28 February 2023
Accepted Manuscript: 29 May 2023